THE JOURNAL OF BIOLOGICAL CHEMISTRY VOL. 288, NO. 17, pp. 11731–11740, April 26, 2013

Quantitative Structural Insight into Human Variegate Porphyria Disease*[S]

Received for publication, February 5, 2013, and in revised form, February 18, 2013 Published, JBC Papers in Press, March 6, 2013, DOI 10.1074/jbc.M113.459768

Baifan Wang[‡1], **Xin Wen**[‡1], **Xiaohong Qin**[§], **Zhifang Wang**[‡], **Ying Tan**[‡], **Yuequan Shen**[§], **and Zhen Xi**[‡2]

From the [‡]*State Key Laboratory of Elemento-Organic Chemistry, Department of Chemical Biology, College of Chemistry, Nankai University, Tianjin 300071, China and the* [§]*College of Life Science, Nankai University, Tianjin 300071, China*

Background: Defects in the human protoporphyrinogen oxidase (PPO) causes the variegate porphyria (VP) disease.
Results: The activity of 44 clinically reported VP-causing mutants have been accurately predicted.
Conclusion: A quantitative understanding into the molecular basis of VP by PPO mutation was established.
Significance: The quantitative insight into VP should be helpful for the diagnosis, precaution, and treatment of this disease.

Defects in the human protoporphyrinogen oxidase (hPPO) gene, resulting in ~50% decreased activity of hPPO, is responsible for the dominantly inherited disorder variegate porphyria (VP). To understand the molecular mechanism of VP, we employed the site-directed mutagenesis, biochemical assays, structural biology, and molecular dynamics simulation studies to investigate VP-causing hPPO mutants. We report here the crystal structures of R59Q and R59G mutants in complex with acifluorfen at a resolution of 2.6 and 2.8 Å. The r.m.s.d. of the Cα atoms of the active site structure of R59G and R59Q with respect to the wild-type was 0.20 and 0.15 Å, respectively. However, these highly similar static crystal structures of mutants with the wild-type could not quantitatively explain the observed large differences in their enzymatic activity. To understand how the hPPO mutations affect their catalytic activities, we combined molecular dynamics simulation and statistical analysis to quantitatively understand the molecular mechanism of VP-causing mutants. We have found that the probability of the privileged conformations of hPPO can be correlated very well with the k_{cat}/K_m of PPO (correlation coefficient, $R^2 > 0.9$), and the catalytic activity of 44 clinically reported VP-causing mutants can be accurately predicted. These results indicated that the VP-causing mutation affect the catalytic activity of hPPO by affecting the ability of hPPO to sample the privileged conformations. The current work, together with our previous crystal structure study on the wild-type hPPO, provided the quantitative structural insight into human variegate porphyria disease.

Protoporphyrinogen oxidase (PPO)[3] (EC 1.3.3.4) is the penultimate enzyme in the heme biosynthetic pathway (1) and catalyzes the oxidation of protoporphyrinogen IX (protogen) to protoporphyrin IX (porphyrin) in the presence of cofactor FAD and molecular oxygen (Fig. 1) (2–4). In humans, defects in the PPO gene, resulting in ~50% decreased activity of PPO, is responsible for the dominantly inherited disorder variegate porphyria (VP) (5–8). VP is a type of acute hepaticporphyria (9–11), which is characterized by an abnormal pattern of porphyrin excretion. VP has been found worldwide (12–15) and is particularly prevalent in the white population of South Africa (~3 in 1000), especially VP caused by the R59W founder mutation (16, 17).

Inhibition of PPO in plants leads the accumulation of protogen, which exports to the cytoplasm and forms porphyrin through nonenzymatic oxidation. The photosensitizing porphyrin can lead to singlet oxygen, which can cause peroxidation of membrane lipids and cell death (18, 19). In human, because the deficiency of PPO leads to the tissue accumulation and excessive excretion of porphyrin, it is hypothesized that the sensitivity of VP patients to light should be similar to the condition in plants (20, 21).

Though the study of VP has been performed for more than half a century (8, 17, 21, 22), the detailed molecular mechanism of VP is still unclear. To address this important issue, we have resolved the crystal structure of human PPO in a resolution of 1.9 Å and characterized 44 VP-causing mutations *in vitro* (22). Based on this high-resolution structure of hPPO and the kinetic data, we attempted to explain the defects of 44 missense mutants. The mapping of these 44 mutations on the hPPO crystal structure indicated these mutants distributed on all of the three structure domains of hPPO. However, our understanding of the molecular mechanism of VP-causing mutants was limited because our insights mostly depend on structural analysis and *in silico* docking (22); the detailed information of molecular motion on substrate binding was especially lacking. In this work, the site-directed mutagenesis, biochemical assays, structural biology, and molecular dynamics simulation studies have been carried out to understand molecular mechanism of VP-causing mutants. We report here the crystal structures of R59Q and R59G mutants in complex with acifluorfen at a resolution of 2.6 and 2.8 Å. However, these highly similar static crystal structures of mutants with the wild-type could not quantitatively explain the observed large differences in their enzymatic

* This work was supported by Ministry of Science and Technology of the People's Republic of China Grants 2010CB126102 and 2011BAE06B05 and National Natural Science Foundation of China Grants 20932005 and 21172122.

The atomic coordinates and structure factors (codes 4IVO and 4IVM) have been deposited in the Protein Data Bank (http://wwpdb.org/).

[S] This article contains supplemental Tables S1–S7 and Figs. S1–S7.

[1] Both authors contributed equally to this work.

[2] To whom correspondence should be addressed: State Key Laboratory of Elemento-Organic Chemistry, Dept. of Chemical Biology, College of Chemistry, Nankai University, No. 94, Weijin Rd., Tianjin, China. Tel.: 86-022-23504782; Fax: 86-022-23504782; E-mail: zhenxi@nankai.edu.cn.

[3] The abbreviations used are: PPO, protoporphyrinogen IX oxidase; MD, molecular dynamics; VP, variegate porphyria; protogen, protoporphyrinogen IX; CPDF, conformation probability density function; PC, privileged conformations; r.m.s.d., root mean square deviation.

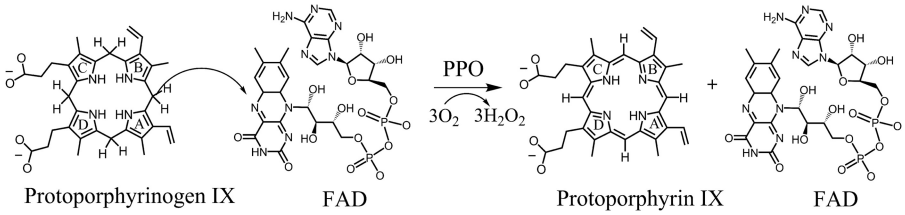

FIGURE 1. **Protoporphyrinogen IX oxidase reaction.**

activity. We further combined molecular dynamics simulation and statistical analysis to quantitatively understand the molecular mechanism of VP-causing mutants. We have found that the VP-causing mutations affect the catalytic activity of hPPO by affecting the ability to sample privileged conformations. The effects of 44 clinically important mutations on the catalytic activity of hPPO have been accurately predicted with $R^2 = 0.94$ in this work.

EXPERIMENTAL PROCEDURES

Plasmid Construction of hPPO Mutants—The recombinant plasmid (pHPPO-X) was a generous gift from Dr. H. A. Dailey (University of Georgia). All mutations of hPPO described here were generated from the recombinant plasmid (pHPPO-X) using DpnI-mediated site-directed mutagenesis methods and confirmed by DNA sequencing.

Expression and Purification of Mutant hPPO—Plasmids of wild-type and various hPPO mutants were initially transformed into BL21(DE3)pLysS *Escherichia coli* cells. The single colony of resulting cells was grown in 10 ml of 2×YT medium with 100 μg/ml ampicillin at 37 °C overnight. Total culture were then inoculated into one liter of 2×YT medium containing 100 μg/ml ampicillin and grown with shaking at 37 °C to A_{600} of 0.6. The expression of the recombinant hPPO wild-type enzyme and its mutants were induced by adding isopropyl 1-thio-β-D-galactopyranoside to a final concentration of 1 mM. Cells were grown for an additional 4 h at 25 °C.

E. coli cells were harvested by centrifugation at 5000 × *g* for 15 min, and the cell pellet was suspended in lysis buffer (20 mM Tris-HCl, pH 8.0, 500 mM NaCl, 10 mM imidazole, 0.5% Triton X-100 (v/v), and 10% glycerol) and disrupted by sonication and lysozyme (0.1 mg/ml). Cellular debris was removed by centrifugation at 20,000 × *g* for 50 min. The supernatant was loaded directly onto a Ni^{2+} nitrilotriacetic acid column, which was pre-equilibrated in lysis buffer, and left at 4 °C for 2 h. The Ni^{2+} nitrilotriacetic acid column was then washed with four column volumes of wash buffer (50 mM NaH_2PO_4 (pH 7.0), 100 mM NaCl, 50 mM imidazole, 0.03% Triton X-100 (v/v) and 10% glycerol). Proteins were eluted with three column volumes of elution buffer (50 mM NaH_2PO_4 (pH 7.0), 100 mM NaCl, 200 mM imidazole, 0.03% Triton X-100 (v/v), and 10% glycerol). The eluted proteins were concentrated to 2.5 ml and loaded onto Superdexs200 size-exclusion column (GE Healthcare) with running buffer (20 mM Tris-HCl, pH 7.0, 200 mM NaCl, 5 mM DTT, 5 mM EDTA, and 0.02% Tween 80 (v/v) (Anatrace)) at a flow rate of 0.3 ml/min. Protein concentration was determined using Bradford method (Bio-Rad).

Enzyme Assay for Kinetic Analysis—PPO activity was assayed by measuring the constant velocity of formation of protoporphyrin IX from protoporphyrinogen IX using a 96-well plate with the continuous fluorometric methods at 25 °C (23–25). The product has a maximum excitation wavelength at 410 nm and a maximum emission wavelength at 630 nm. The total volume of the reaction mixture was 200 μl consisting of 0.1 M potassium phosphate buffer (pH 7.4), 5 μM FAD, 5 mM DTT, 1 mM EDTA, 0.2 M imidazole, and 0.03% Tween 80 (v/v). The enzymatic reaction was started by the addition of substrate. The autoxidation rates were determined concomitantly and were subsequently subtracted. Kinetic parameters, including the Michaelis-Menten constant (K_m), the maximal velocity (V_{max}), and the catalytic constant (k_{cat}), were determined by a Lineweaver-Burk plot.

Crystallization and Data Collection—Crystals of the mutant hPPOs·acifluorfen complexes were grown using the same method as the wild-type protein described previously (22). Diffraction data were collected on beam station BL17U1 of the Shanghai Synchrotron Radiation Facility. The data of R59Q and R59G were processed and scaled to 2.6 and 2.8 Å, respectively, using the HKL2000 software package (26). The crystals of the complex of mutant hPPO with acifluorfen belong to the space group *R*3.

Structure Determination and Refinement—The initial phases were obtained by molecular replacement using the structure of PPO enzyme from *Homo sapiens* (Protein Data Bank code 3NKS (22)) as a template. The program PHASER was able to locate one molecule in the asymmetric unit (27). The models were built manually using the program COOT (28) and refined using the program CNS (29) and Phenix. The final structure of R59Q mutant had an R_{cryst} value of 17.9% and an R_{free} value of 24.3%. The Ramachandran plot calculated by the program PROCHECK (30) showed that 90.3% of the residues were in their most favored regions, 9.7% of the residues were in additionally allowed regions, and no residues were in generously allowed regions and disallowed regions. The structure of R59G mutant had an R_{cryst} value of 17.5% and an R_{free} value of 24.4%. The Ramachandran plot calculated by the program PROCHECK (30) showed that 89.2% of the residues were in their most favored regions, 10.5% of the residues were in additionally allowed regions, 0.3% of the residues were in generously allowed regions, and no residues disallowed regions. Detailed data collection and refinement statistics are summarized in supplemental Table S1.

Molecular Dynamics Simulations—MD simulations for wild-type and mutant hPPO in complexes with substrate protogen were carried out to generate the equilibrium conformations for each of the studied systems. The crystal structures of the wild-type hPPO (Protein Data Bank code 3NKS (22)) and R59G and

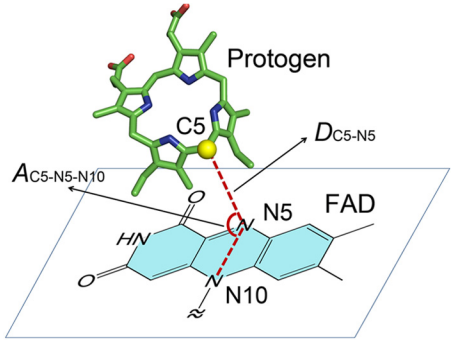

FIGURE 2. **A schematic description of the $D_{C5\text{-}N5}$ and $A_{C5\text{-}N5\text{-}N10}$ used as a set of geometry parameters to represent the conformation of reactants protogen and FAD.** FAD was shown on the isoalloxazine plane only.

R59Q mutants were taken as the starting point for MD simulations of the complexes. All missing residues of the structure were added using InsightII (Accelrys, Inc., San Diego, CA). The hydrogen atoms were added to hPPO structure using leap module of AMBER (version 9) (31). The structures of other hPPO mutants were generated from the structure by mutation of corresponding residues using InsightII (Accelrys, Inc.). A 3000-step minimization was performed on the mutated residues and the adjacent residues within 4.0 Å from the mutated residue to remove the steric clash. The optimization were performed with SANDER module of AMBER (version 9) (31) and AMBER (version 03) force fields (32, 33).

The coordinates of protogen were taken from the previous docking studies where protogen was docked into the crystal structure of hPPO (22). The force field parameters of cofactor FAD and protogen were generated with the Gaussian 03 (34) and AMBER (version 9).

Each of the complex systems was immersed in a truncated octahedral box of explicit TIP3P water molecules and was neutralized by adding counter ions (Cl^- or Na^+). All MD simulations were carried out with the SANDER module of AMBER (version 9) (31). Prior to MD simulations, the molecular systems were subjected to a series of energy minimizations to relax the system. In MD simulations, particle mesh Ewald (35) and periodic boundary condition were employed to deal with the long range electrostatic interactions. The SHAKE method (36) was used to constrain bonds involving hydrogen atoms to tolerate 2-fs time steps. The system was gradually heated from 0 to 300 K over 50 ps. Equilibrating calculation was executed at 1 atm and at 300 K for 50 ps. Then, 5-ns MD simulations were performed under 300 K and 1 atm. The snapshot of the system was taken every 1 ps. Trajectories of reactants protogen and FAD after the initial 2 ns of equilibration were considered for analysis; thus, 3000 MD structures, collected during the time period of 2001–5000 ps, were generated for each of the systems using the ptraj module of AMBER (version 9). To test the consistency of data from MD simulations, the simulation of wild-type hPPO system was extended to 44 ns.

Description of the Conformational Space of the Reactants—Based on the proposed PPO catalytic mechanism (4, 37) and our previous study (22), the distance between C5 atom of protogen and N5 atom of FAD ($D_{C5\text{-}N5}$) and the angle between C5, N5 and N10 ($A_{C5\text{-}N5\text{-}N10}$) (shown in Fig. 2) as geometry parameters were used to describe the reactant conformational space. Each conformation of the reactants was represented by a pair of $D_{C5\text{-}N5}$-$A_{C5\text{-}N5\text{-}N10}$. For each of the studied systems, conformational ensemble of the reactants was represented by a set of $D_{C5\text{-}N5}$-$A_{C5\text{-}N5\text{-}N10}$ pairs, corresponding to a set of discrete data points in a $D_{C5\text{-}N5}$-$A_{C5\text{-}N5\text{-}N10}$ plane.

Construction of Conformation Probability Density Function (CPDF)—To calculate the probability of the reactant conformation in any given interval of $D_{C5\text{-}N5}$ and $A_{C5\text{-}N5\text{-}N10}$, for each of the studied systems, we converted the sets of discrete data points of $D_{C5\text{-}N5}$-$A_{C5\text{-}N5\text{-}N10}$ pairs to the CPDF, denoted as $Z(A,D)$. The conversion was performed in the following steps: (i) dividing the $D_{C5\text{-}N5}$-$A_{C5\text{-}N5\text{-}N10}$ plane into square bins with 0.1 Å width and 5° length; (ii) taking count of the number of data points for each bin; (iii) calculating the density of each bin by the number of $D_{C5\text{-}N5}$-$A_{C5\text{-}N5\text{-}N10}$ data points fall in the corresponding bin being divided by the total number of the angle-distance data points; (iv) fitting the data with the two-dimensional Gaussian function to construct $Z(A,D)$ by the non-linear surface fitting methods implemented in Origin Lab (version 8.0, Northampton, MA). The general form of the CPDF can be presented as follows in Equation 1,

$$Z(A,D) = C_{\exp}\left\{-\frac{1}{2}\left(\frac{A-\mu_A}{\sigma_A}\right)^2 - \frac{1}{2}\left(\frac{D-\mu_D}{\sigma_D}\right)^2\right\} \quad \text{(Eq. 1)}$$

where Z denotes the conformation probability density in $D_{C5\text{-}N5}$ and $A_{C5\text{-}N5\text{-}N10}$ for the observing systems. The factor C in this expression ensures that the total area under the curve $Z(A,D)$ is equal to one. The parameter μ is called the mean of the normal distribution, and it determines the coordinate of highest point of the Gaussian surface. The parameter σ is called the S.D. and describes how concentrated the distribution is around its mean.

Calculation of the Probability of PC—The probability of any conformation of the reactants at equilibrium was calculated by taking the integral of the CPDF over the given integration intervals. Based on the x-ray structures of the flavoenzyme complexes with substrate analogues (38), we defined the conformations with $D_{C5\text{-}N5}$ within 3.0–3.8 Å and $A_{C5\text{-}N5\text{-}N10}$ within 96–117° as the privileged conformations (PC). For each studied system, the probability of PC, denoted P_{PC}, was calculated by the bivariate integration of corresponding CPDF over the interval (96, 117) for $A_{C5\text{-}N5\text{-}N10}$, and (3.0, 3.8) for $D_{C5\text{-}N5}$ (Equation 2) using Matlab software (The Math Works, Natick, MA). The general integral form was expressed as follows,

$$P_{PC} = \int_{A_2}^{A_1}\int_{D_2}^{D_1} C_{\exp}\left\{-\frac{1}{2}\left(\frac{A-\mu_A}{\sigma_A}\right)^2 - \frac{1}{2}\left(\frac{D-\mu_D}{\sigma_D}\right)^2\right\} dA\,dD \quad \text{(Eq. 2)}$$

Correlation of the P_{PC} with the k_{cat}/K_m of PPO Mutants—Nonlinear regression analyses were performed in Origin Lab (version 8.0) to explore whether the P_{PC} for the studied systems could be correlated with corresponding k_{cat}/K_m values. Best fitting was assessed by correlation coefficient, square root of mean square error, and F-test comparisons.

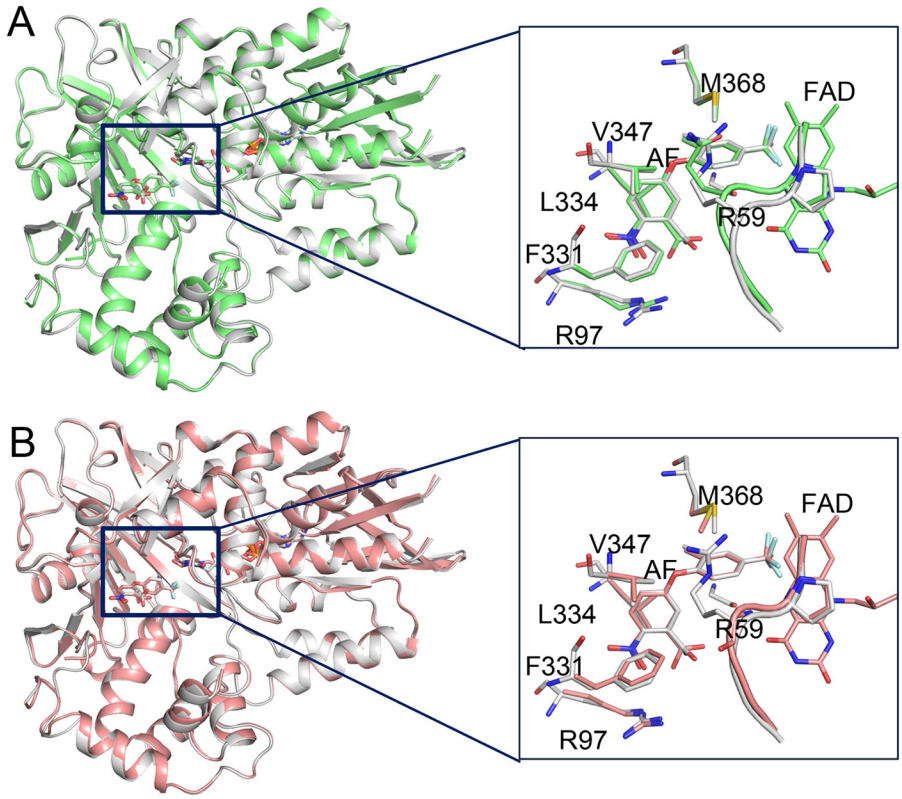

C

Kinetic data and crystal structural deviation for wild-type hPPO and R59 mutants

Mutant	K_M (μM)	k_{cat} (min^{-1})	k_{cat}/K_M (μM^{-1} min^{-1})	Relative fold	Crystal resolution (Å)	Overall structure RMSD with wild-type (Å)	Active site structure RMSD with wild-type (Å)
Wild-type	2.33	6.14	2.63	100.00%	1.9	0.00	0.00
R59Q	13.3	3.69	0.28	10.55%	2.6	0.26	0.20
R59G	3.31	2.48	0.75	25.53%	2.8	0.29	0.15

FIGURE 3. **Comparison of the crystal structures and activities of the wild-type hPPO and R59Q and R59G mutants.** *A*, comparison of the overall (*left panel*) and active site (*right panel*) of the wild-type and R59Q mutant structure. *B*, comparison of the overall (*left panel*) and active site (*right panel*) of the wild-type and R59G mutant structure. Wild-type is shown in *white*, R59Q is shown in *green*, and R59G is shown in *salmon*. *C*, kinetic data and crystal structural deviation for wild-type hPPO and Arg-59 mutants.

Accession Codes—Coordinates and associated structure factors of solved structures for human protoporphyrinogen IX oxidase R59Q and R59G mutants in complex with acifluorfen have been deposited in the Protein Data Bank (codes 4IVO and 4IVM, respectively).

RESULTS AND DISCUSSION

Crystal Structure of R59Q and R59G Mutant—The R59W mutation is by far the most prevalent VP-causing mutation identified, and >94% of the patients in South Africa carry this mutation (16, 17). Biochemical studied showed that the R59W mutation dramatically decreased the catalytic constant of hPPO *in vitro* (17, 21, 41, 42). Herein, we have determined the crystal structures of R59Q and R59G mutants in complex with acifluorfen at a resolution of 2.6 and 2.8 Å, respectively, with 1 molecule/asymmetric unit. Data collection and refinement statistics appear in supplemental Table S1.

Overall, the structures of R59Q, R59G, and wild-type hPPO were highly similar, with r.m.s.d. in Cα positions of 0.26 and 0.29 Å, respectively (Fig. 3, *A* and *B*). The mutation caused minor structural change in the active site residues. The r.m.s.d. of the active site residues (residues within 4.0 Å distance with acifluorfen) of R59Q and R59G mutants with wild-type was 0.20 and 0.15 Å, respectively. In addition, after being subjected to the molecular dynamics simulation with bound substrate, the r.m.s.d. of the active site residues of R59Q and R59G mutants with wild-type was 0.27 and 0.39 Å, respectively. These data suggested that the static active site architecture was not significantly affected by the mutations (Fig. 3, *A* and *B*). These highly similar static crystal structures of mutants with the wild-type could not quantitatively explain the observed large differences in their enzymatic activity (Fig. 3*C*). To answer the question how the hPPO mutations affect their catalytic activities, the dynamics motion of the structure of hPPO mutants should be considered.

Conformational Distribution of the Reactants—Dynamics simulation methods are widely used to obtain information on the time evolution of conformations of proteins and other biological macromolecules, which present a powerful complement

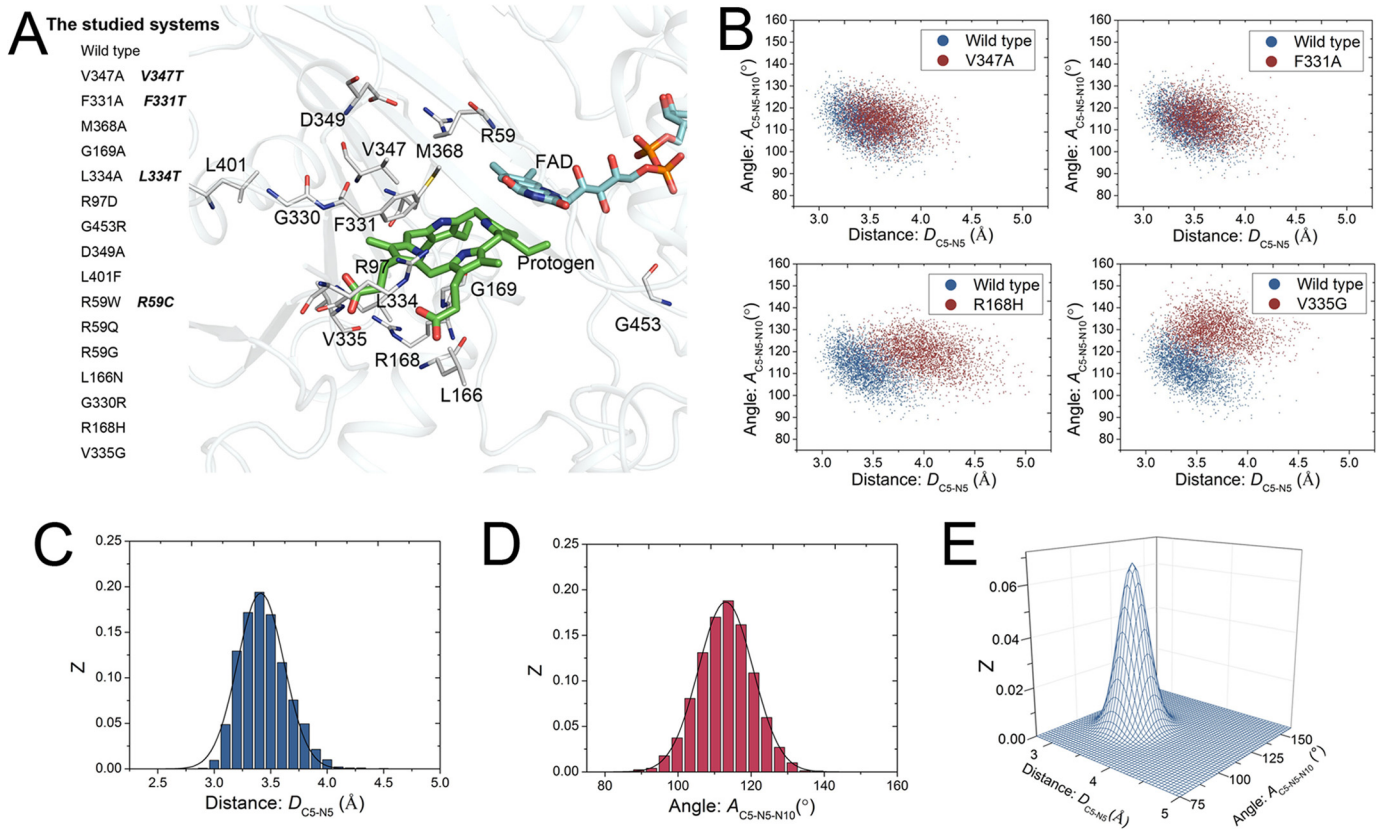

FIGURE 4. **Conformation probability analysis of the PPO mutants.** *A*, A total of 17 mutants listed at left column were used to construct the prediction model, and four mutants shown at the *right column* were the mutants constructed and measured later as the initial test set. The mutated residues, the cofactor FAD, and the substrate protogen were shown in stick representation with *gray*, *cyan*, and *green* carbon atoms, respectively. *B*, $D_{C5\text{-}N5}$ *versus* $A_{C5\text{-}N5\text{-}N10}$ scatter plots. The distribution of the pairs of $D_{C5\text{-}N5}$-$A_{C5\text{-}N5\text{-}N10}$ for wild-type hPPO from MD simulation was shown in *blue*, and the distributions for the mutants were shown in *red*. *C*, probability distribution of $D_{C5\text{-}N5}$ observed for wild-type hPPO. Horizontal coordinates indicate $D_{C5\text{-}N5}$ value; vertical coordinates indicate probability density. *D*, probability distribution of $A_{C5\text{-}N5\text{-}N10}$ observed for wild-type hPPO. Horizontal coordinates indicate $A_{C5\text{-}N5\text{-}N10}$ value; vertical coordinates indicate probability density. *E*, conformation probability density function surface for wild-type hPPO.

to static structures of proteins and other biomolecules. Convergence of results from simulation with experimental data provides a foundation for using simulations to enhance experimental observations and study features of biomolecules that cannot be seen directly in experiments. Because it was difficult to study the effect of the mutants only from the comparison of the crystal structures of wild-type and mutant hPPO, we have therefore chosen to study the molecular mechanism of how VP-causing mutants affect the activity of hPPO through molecular dynamics simulations of the hPPO·substrate complex. First, we chose wild-type hPPO and 16 hPPO mutants (including the R59G and R59Q mutants) as the studied systems (Fig. 4*A*), because all of these mutations are involved in the binding of substrate or FAD and clinically found in the VP patients (7, 9–11). MD simulations for the 17 enzymes in complexes with substrate protogen were carried using AMBER (version 9) (31). For each of the studied system, 3000 conformers extracted from the MD trajectory during the time period of 2001–5000 ps were used as the reduced representation of the conformational ensemble at equilibrium state.

For each studied system, the fluctuations of temperature, density, and total energy during the MD simulation were examined, and the r.m.s.d. of the backbone heavy atoms with respect to the starting structures were reported as a function of time. These physical quantities from the wild-type hPPO system were shown in supplemental Fig. S1. Other detailed data about the MD trajectories of studied systems were provided in supplemental Figs. S2 and S3 and supplemental Table S2).

It was essential to describe conformational space of the reactants using a set of proper parameters for capturing the salient features of conformational distribution of the reactants at equilibrium system. The oxidation of protogen to protoporphyrin IX catalyzed by PPO involves the rupture of C-H bond of methylene of macrocycle in protogen, coupled to the transfer of two electrons to FAD (4). The carbon atoms involved in these C-H bonds were considered as the sites of oxidative attack, and N5 of the tricyclic isoalloxazine ring system of FAD was believed to take part directly in substrate dehydrogenation (37, 43–45). In the previous studies, we also explored the binding mode of protogen at the active site of hPPO based on the high-resolution crystal structure of hPPO by the molecular docking, MD simulation, and quantum mechanical calculations. Our studies indicated that the methylene bridge C5 atom of protogen (see Fig. 2) was close to the N5 atom of FAD (22). Thus, the distance between C5 and N5 atoms ($D_{C5\text{-}N5}$) and the angle between C5, N5, and N10 ($A_{C5\text{-}N5\text{-}N10}$) (shown in Fig. 2) as a set of geometry parameters were used to describe the conformational space in the reaction process. In conformational ensembles, each conformation of the reactants (protogen and FAD) was represented by a pair of $D_{C5\text{-}N5}$-$A_{C5\text{-}N5\text{-}N10}$, whereas each conforma-

TABLE 1
The parameters of the conformation probability density functions, the kinetic data, and the P_{PC} for each of the studied systems

Enzyme	R^2	C	μ_A	σ_A	μ_D	σ_D	K_m	k_{cat}	k_{cat}/K_m	$k_{cat}/K_{m(pred)}$ [a]	P_{PC}
							μM	min^{-1}	$min^{-1}\ \mu M^{-1}$	$min^{-1}\ \mu M^{-1}$	
Wild-type	0.92	0.12	113.33	7.16	3.41	0.19	2.33	6.14	2.63	2.46	0.66
V347A	0.97	0.12	114.53	6.39	3.60	0.20	2.61	3.70	1.42	1.33	0.54
F331A	0.96	0.10	115.13	6.95	3.56	0.23	3.41	4.44	1.30	1.31	0.51
M368A	0.95	0.08	102.67	8.82	3.67	0.21	3.16	3.95	1.25	1.36	0.53
G169A	0.99	0.11	117.12	7.16	3.55	0.20	5.26	5.02	0.95	0.74	0.44
L334A	0.98	0.11	126.00	7.62	3.39	0.18	3.93	1.40	0.36	0.09	0.12
R97D	0.94	0.07	126.11	8.65	3.65	0.27	7.79	2.35	0.30	0.07	0.11
G453R	0.98	0.10	124.75	8.69	3.30	0.19	3.87	0.99	0.26	0.18	0.18
D349A	0.96	0.12	126.48	8.23	3.30	0.17	3.09	0.65	0.21	0.12	0.12
R59G	0.97	0.09	121.80	8.06	3.50	0.21	3.31	2.48	0.75	0.27	0.25
R59Q	0.94	0.04	111.45	8.34	3.99	0.44	13.30	3.69	0.28	0.26	0.23
R59W	0.94	0.08	124.51	7.14	3.63	0.28	4.21	0.74	0.18	0.11	0.10
L401F	0.98	0.12	119.46	7.23	3.42	0.18	6.79	0.95	0.14	0.52	0.36
L166N	0.95	0.11	120.23	8.00	3.34	0.19	6.79	0.75	0.11	0.43	0.33
G330R	0.98	0.14	121.51	7.15	3.32	0.16	8.13	0.76	0.09	0.27	0.26
R168H	0.95	0.08	119.63	6.92	3.96	0.28	11.82	0.71	0.06	0.07	0.10
V335G	0.97	0.09	129.85	7.07	3.64	0.26	1.10	0.06	0.05	0.01	0.02

[a] k_{cat}/K_m value was predicted by Equation 3.

tional ensemble of the reactants was represented by a set of $D_{C5\text{-}N5}$-$A_{C5\text{-}N5\text{-}N10}$ pairs, corresponding to a set of discrete data points in a $D_{C5\text{-}N5}$-$A_{C5\text{-}N5\text{-}N10}$ plane.

In Fig. 4*B*, the $D_{C5\text{-}N5}$-$A_{C5\text{-}N5\text{-}N10}$ pairs as data points were plotted in a $D_{C5\text{-}N5}$-$A_{C5\text{-}N5\text{-}N10}$ plane, in which each of the scatter plots for the mutants was superposed on the one for wild-type system to compare the conformational spaces of the reactants of wild-type hPPO and mutants. The $D_{C5\text{-}N5}$ *versus* $A_{C5\text{-}N5\text{-}N10}$ scatter plots for the mutants were provided in supplemental Fig. S4. The ranges of $D_{C5\text{-}N5}$ and $A_{C5\text{-}N5\text{-}N10}$ and the average of the two values for each conformational ensemble were listed in supplemental Table S3.

From the pairs of $D_{C5\text{-}N5}$-$A_{C5\text{-}N5\text{-}N10}$ scatter plots, we obtained the qualitative understanding of the conformational distribution for each of the studied system. As seen in Fig. 4*B* and supplemental Table S3, despite the fact that the wild-type, V347A, and F331A system had similar regions where the data points appeared, the data pattern was different for other studied systems. The studied systems with higher catalytic efficiency, for example, wild-type hPPO and F331A, showed more condensed data distribution than that of the systems with lower catalytic efficiency. The results suggested that the catalytic efficiency may be related to the conformational distribution of reactants for our studied systems.

As an estimate of the probability distribution of a continuous variable, the histograms of probability of $D_{C5\text{-}N5}$ and $A_{C5\text{-}N5\text{-}N10}$ were investigated for each of the studied systems. Of these, the histograms for the wild-type hPPO, as an example, were displayed in Fig. 4, *C* and *D*, in which a bell-shaped probability distributions were observed for both of $D_{C5\text{-}N5}$ and $A_{C5\text{-}N5\text{-}N10}$. The same behaviors were also observed in all of the mutants. For all of the studied systems, the probability distributions of $D_{C5\text{-}N5}$ and $A_{C5\text{-}N5\text{-}N10}$ were well approximated by Gaussian distributions, with R^2 of 0.95–0.99 for $D_{C5\text{-}N5}$, and 0.99 for $A_{C5\text{-}N5\text{-}N10}$, respectively (supplemental Table S4 and supplemental Fig. S5).

The scattered $D_{C5\text{-}N5}$-$A_{C5\text{-}N5\text{-}N10}$ data were converted for each of the studied systems to a continuous function of random variables $D_{C5\text{-}N5}$ and $A_{C5\text{-}N5\text{-}N10}$, $Z(D_{C5\text{-}N5}, A_{C5\text{-}N5\text{-}N10})$, namely the CPDF, by two-dimensional histogram technique. Considering that both of distribution of $D_{C5\text{-}N5}$ and $A_{C5\text{-}N5\text{-}N10}$ for each studied system followed Gaussian distribution, we fitted the binned data of $D_{C5\text{-}N5}$-$A_{C5\text{-}N5\text{-}N10}$ to a two-dimensional Gaussian distribution using a nonlinear regression implemented in Origin Lab (version 8.0). For all of the 17 studied systems, they were well approximated by Gaussian distributions (Equation 1), and the best estimates of the mean and standard deviation obtained from the fitting procedures for each of studied systems were reported in Table 1. The CPDF surface for the wild-type and mutant hPPO were displayed in Fig. 4*E* and supplemental Fig. S6.

The Probability of the PC—Based on the x-ray crystal structures of the flavoenzyme complexes with substrate analogues, Fraaije and Mattevi (38) have studied the catalytic features of the flavoenzymes that perform a dehydrogenation reaction. The studies indicated that the geometry parameters between substrate and FAD corresponding to the distance $D_{C5\text{-}N5}$ and the angle $A_{C5\text{-}N5\text{-}N10}$ of hPPO were generally conserved for the studied flavoenzymes, within 3.0–3.8 Å for $D_{C5\text{-}N5}$, 96 to 117° for $A_{C5\text{-}N5\text{-}N10}$. Therefore, we defined the conformations with both of $D_{C5\text{-}N5}$ within 3.0–3.8 Å and $A_{C5\text{-}N5\text{-}N10}$ within 96–117° as the PC. In fact, there is widely accepted proposition that the reactant particles must collide with appropriate orientations to achieve an enzymatic reaction, and enzymes bind to their substrates for the formation of a substrate·enzyme complex prior to the reaction step. Here, we quantify the appropriate orientation collision probability between the reactants as the P_{PC}, which was obtained by the bivariate integration of the CPDF over the reactable geometry ranges. Such a quantitation may correlate with the catalytic activity of enzymes.

For each of 17 studied systems, the probability of reactant conformation in any given interval of $D_{C5\text{-}N5}$ and $A_{C5\text{-}N5\text{-}N10}$ can be calculated through the corresponding CPDF. Thus, P_{PC} was calculated by the bivariate integration of the corresponding CPDF over the interval (96, 117) for $A_{C5\text{-}N5\text{-}N10}$, and (3.0, 3.8) for $D_{C5\text{-}N5}$ using Matlab software (supplemental Fig. S7). P_{PC} for each of the studied systems were listed in Table 1. The kinetic parameters of the wild-type hPPO and 16 mutants were also listed in Table 1. It can be found that P_{PC} of each studied system goes the same trend with the k_{cat}/K_m of enzyme

mutants, which is in keeping with our first hypothesis that the probability of the appropriate orientated collision between the reactants should correlate with the catalytic activity of enzymes.

Correlation of the Probability of PC with the Catalytic Efficiency of the Enzymes—The k_{cat}/K_m values of 17 studied systems were plotted against the corresponding P_{PC} values. Upon inspection of Fig. 5*A*, we found that the P_{PC} increased with a nonlinear increasing of the k_{cat}/K_m. Thus, the paired data were fitted to BoxLucas1 functions, and the best fit was assessed by square root of mean square error values and *F*-test comparisons in Origin Lab (version 8.0). Finally, the correlation equation with $R^2 = 0.90$, square root of mean square error = 0.22, and $F = 140.82$ was expressed as follows in Equation 3.

$$k_{cat}/K_M = 0.11(e^{4.84P_{PC}} - 1) \quad \text{(Eq. 3)}$$

The predicted values of the k_{cat}/K_m from this regression were listed in Table 1. The experimental k_{cat}/K_m values are plotted against the predicted k_{cat}/K_m in Fig. 5*B* with correlation $R^2 = 0.91$. The relatively high R^2 between the experimental and predicted k_{cat}/K_m indicated that a high proportion of the data can be explained by Equation 3. Thus, these mutants affect the catalytic activity of hPPO by affecting the P_{PC}. Four more mutants such as F331T, L334T, R59C, and V347T have thus been constructed, and kinetics have been measured to test our model. Their experimental k_{cat}/K_m values again correlated very well with the calculated values (Fig. 5*C* and supplemental Table S5), which further indicated that the probability of the privileged conformations in the PPO-catalyzed reaction process made the major contribution. Encouraged by these results, we decided to use this computational approach to predict the catalytic activities of all clinically reported VP-causing mutants.

The Molecular Mechanism of the VP-causing Mutants—The mapping of these 44 VP-causing mutants on the hPPO crystal structure indicated these mutants distributed on all of the three structure domains of hPPO (Fig. 6*A*). We categorized these mutants into five potential categories, *i.e.* affecting the substrate binding, FAD binding, hydrophobic core, secondary structure, and surface of hPPO. However, our understanding of the molecular mechanism of VP-causing mutants was limited because our insights mostly depend on the static structural analysis and *in silico* docking. In this work, based on molecular dynamics simulation and statistical analysis, we found the positive correlation of the P_{PC} with k_{cat}/K_m of the 17 PPO variants. We set out to further test whether the VP-causing mutants affect the catalytic activity of hPPO by affecting the distribution of PC. Among the 44 mutants, 36 mutants display detectable activity, whereas eight mutants were inactive. (The catalytic activity of the inactive mutants was designated as zero.) The k_{cat}/K_m values of these mutations were then predicted using the Equation 3, and the data were listed in supplemental Table S4. Fig. 6*B* depicts a correlation plot of the predicted and experimental k_{cat}/K_m values, in which the correlation coefficient (R^2) is 0.94.

Because the quantitative correlation between experimental k_{cat}/K_m and the computational P_{PC} could be established, we can therefore assess the molecular mechanism of the VP disease by

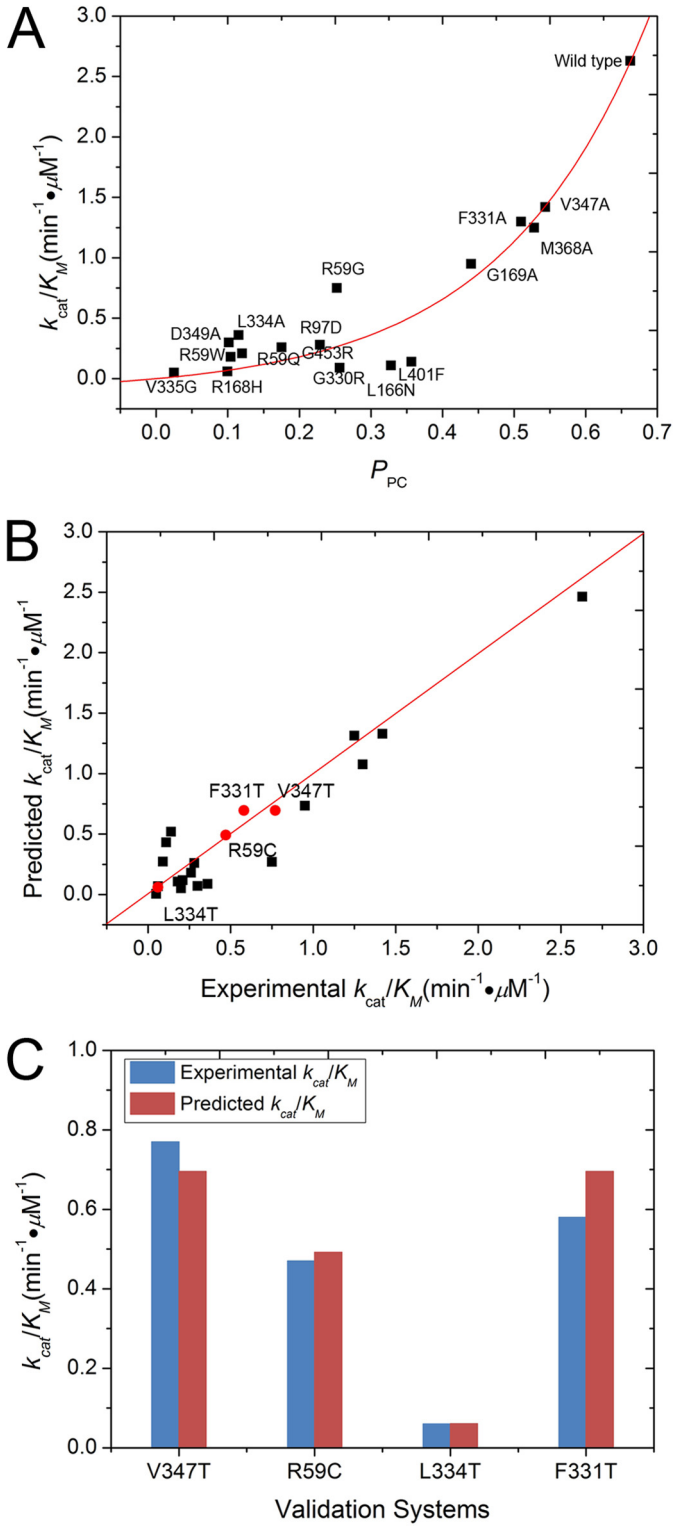

FIGURE 5. **Correlating the probability of PC with the catalytic efficiency of enzymes.** *A*, plot of the experimental values of k_{cat}/K_m values *versus* the corresponding P_{PC} for the 17 studied systems, the exponential correlation was shown as a *red line* with the R^2 of 0.90. *B*, plot of the experimental and predicted k_{cat}/K_m for all studied systems from the Equation 3. *Black squares* indicate 17 studied systems that were used to generate the Equation 3; *red dot* indicates four mutants for experimental validation. The *diagonal red line* corresponding to $(k_{cat}/K_m)_{exp} = (k_{cat}/K_m)_{pred}$ was provided for visual guidance with the R^2 of 0.91. *C*, comparison of the experimental (in *blue*) and predicted (in *red*) k_{cat}/K_m value for the test mutants of hPPO.

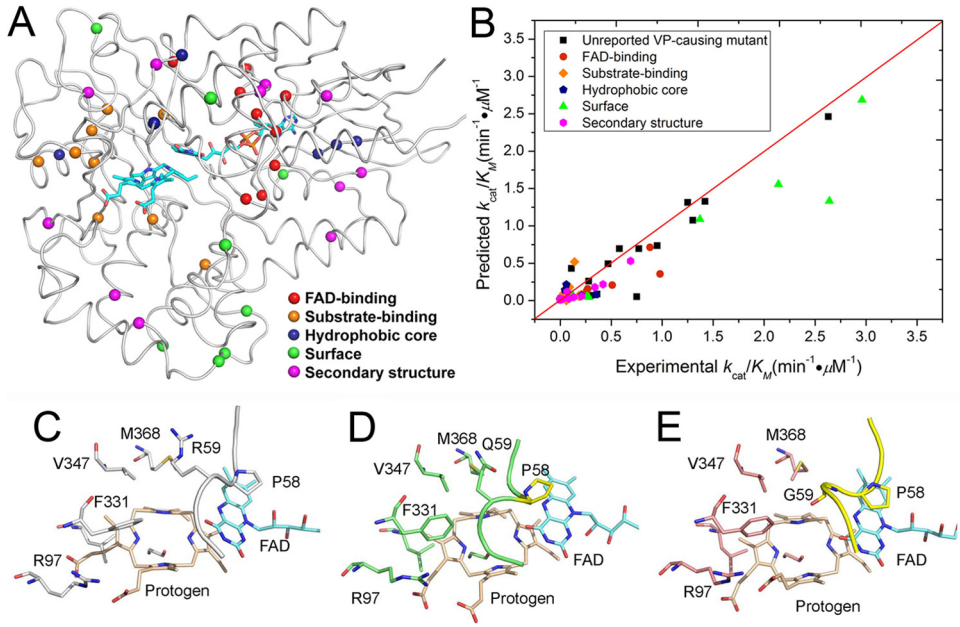

FIGURE 6. **Prediction of the catalytic activity and molecular mechanism of VP-causing mutants.** *A*, the mapping of the VP-causing mutations on the crystal structure of hPPO. Mutants are indicated by *colored spheres*, substrate and FAD are shown in stick representation. *B*, plot of the experimental and predicted k_{cat}/K_m for the clinically reported or potential VP-causing mutants from the Equation 3. The data points are colored by their effects on the activity of hPPO. The *diagonal red line* corresponding to $(k_{cat}/K_m)_{exp} = (k_{cat}/K_m)_{pred}$, the correlation showed $R^2 = 0.94$. *C*, the average conformation of the active site from dynamics simulation for the wild-type. *D*, the average conformation of the active site from dynamics simulation for R59Q. *E*, the average conformation of the active site from dynamics simulation for R59G.

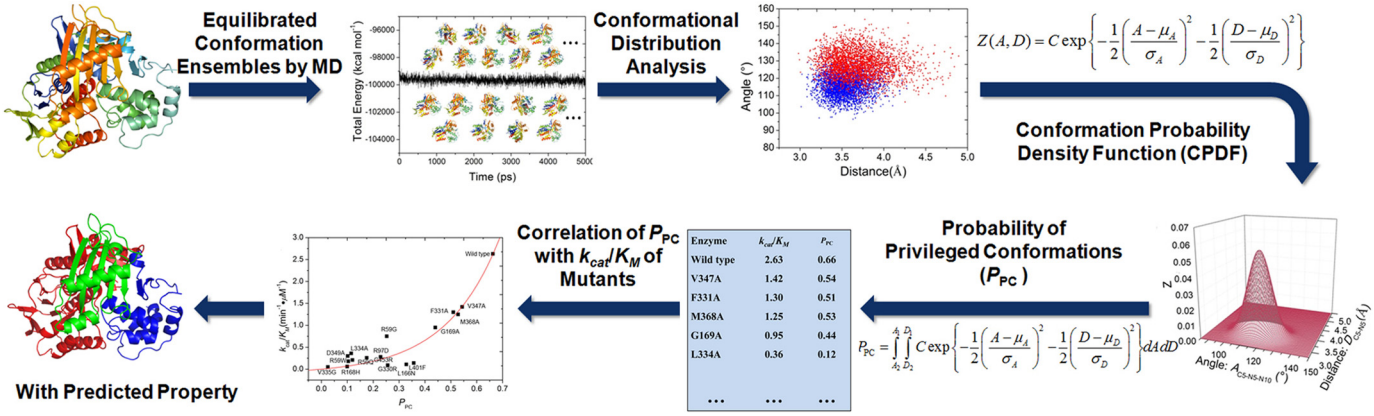

FIGURE 7. **Prenzyme: a protocol for predicting mutant enzyme properties through MD/conformational distribution statistical analysis.**

VP-causing mutants from dynamics simulation. Based on our molecular dynamics simulation and statistical analysis, we found that the VP-causing mutations, even those far from the active site and FAD could significantly impact the P_{PC} of hPPO. These mutations lead to the changes of structural and conformational motions of the entire hPPO that alter the ability of sampling privileged conformations, thereby affecting the catalytic activity of hPPO. Now we can quantitatively understand how the catalytic activities were affected by hPPO mutations, a result cannot come out of the static crystal structure of hPPO mutants.

From dynamics simulation, it could be seen that in the wild-type, the side chain of Pro-58 is stacking with the isoalloxazine ring of FAD, and the average distance of all simulated ternary conformations between the side chain center of Pro-58 and the center of ring B of isoalloxazine ring of FAD was kept at ~3.98 Å during the simulation. While in the R59Q mutant, the average distance increased to 5.43 Å (Fig. 6, *C* and *D*), which indicated that the stacking interaction between Pro-58 and FAD is disrupted in the reaction process by the mutation. In the dynamics simulation of R59G mutants, the average r.m.s.d. of 1.24 Å for the loop of Leu-56–Ile-61 of R59G respect to wild-type (higher than the overall structure r.m.s.d., 0.78 Å) indicated that the loop of Leu-56–Ile-61 undergo a large structural motion compared with the wild-type in the reaction process (Fig. 6, *C* and *E*). Because this loop locates above the isoalloxazine ring of FAD, the structural motion of this loop should affect the binding of the isoalloxazine ring of FAD and therefore affect the activity of PPO. The detailed information from molecular dynamics study about the effects of the clinically reported mutations on enzymatic activity were provided in supplemental Table S7. These data indicated that the VP-causing mutations affect the catalytic activity of hPPO by affecting the ability to sample privileged conformations, which is in accord-

ance with the widely accepted proposition that the reactant particles must collide with appropriate orientations to achieve an enzymatic reaction.

Computational Approach for Predicting the Catalytic Efficiency of Enzyme Mutants—Many reports have shown that an enzyme activity depends on the conformational distribution of reactants in enzyme active site (39, 40, 46–53). In this study, we have shown that the probability of the reactable conformations of reactants could be employed to quantitatively predict the catalytic efficiency of the hPPO mutants. This protocol for predicting catalytic efficiency of mutant hPPO by combining MD simulation/statistical analysis was called Prenzyme (Fig. 7). The protocol was based on the notion that a reaction can occur only through the collisions by the reactants with the privileged conformations, and this favorable collision can be evaluated by the probability of the privileged conformations of ternary catalytic complex. The conformation probability density function can be obtained from statistical analysis of the conformational distribution of the ternary catalytic complex from MD and then gives the probability value by bivariate integration over the intervals of the corresponding geometric parameters of the privileged conformations. The obtained probability should be correlated with k_{cat}/K_m of enzyme mutants.

Acknowledgments—The computation was carried out at National Supercomputer Center in Tianjin, and the calculations were performed on TianHe-1(A). We are grateful to the staff at beamline BL-17U1 in the Shanghai Synchrotron Radiation Facility for excellent technical assistance during data collection.

REFERENCES

1. Matringe, M., Camadro, J. M., Block, M. A., Joyard, J., Scalla, R., Labbe, P., and Douce, R. (1992) Localization within chloroplasts of protoporphyrinogen oxidase, the target enzyme for diphenylether-like herbicides. *J. Biol. Chem.* **267,** 4646–4651
2. Dailey, T. A., and Dailey, H. A. (1996) Human protoporphyrinogen oxidase: expression, purification, and characterization of the cloned enzyme. *Protein Sci.* **5,** 98–105
3. Poulson, R., and Polglase, W. J. (1975) The enzymic conversion of protoporphyrinogen IX to protoporphyrin IX. Protoporphyrinogen oxidase activity in mitochondrial extracts of *Saccharomyces cerevisiae*. *J. Biol. Chem.* **250,** 1269–1274
4. Dailey, H. A. (1990) *Biosynthesis of Heme and Chlorophylls*, pp. 287–391, McGraw-Hill, New York
5. Meissner, P. N., Day, R. S., Moore, M. R., Disler, P. B., and Harley, E. (1986) Protoporphyrinogen oxidase and porphobilinogen deaminase in variegate porphyria. *Eur. J. Clin. Invest.* **16,** 257–261
6. Deybach, J. C., de Verneuil, H., and Nordmann, Y. (1981) The inherited enzymatic defect in porphyria variegata. *Hum. Genet.* **58,** 425–428
7. Brenner, D. A., and Bloomer, J. R. (1980) The enzymatic defect in variegate prophyria. Studies with human cultured skin fibroblasts. *N. Engl. J. Med.* **302,** 765–769
8. Meissner, P. N., Corrigall, A. V., and Hift, R. J. (2012) Fifty years of porphyria at the University of Cape Town. *S. Afr. Med. J.* **102,** 422–426
9. Elder, G. H., Hift, R. J., and Meissner, P. N. (1997) The acute porphyrias. *Lancet* **349,** 1613–1617
10. Kauppinen, R. (2005) Porphyrias. *Lancet* **365,** 241–252
11. Puy, H., Gouya, L., and Deybach, J. C. (2010) Porphyrias. *Lancet* **375,** 924–937
12. Schneider-Yin, X., Harms, J., and Minder, E. I. (2009) Porphyria in Switzerland, 15 years experience. *Swiss Med. Wkly.* **139,** 198–206
13. Di Pierro, E., Ventura, P., Brancaleoni, V., Moriondo, V., Marchini, S., Tavazzi, D., Nascimbeni, F., Ferrari, M. C., Rocchi, E., and Cappellini, M. D. (2009) Clinical, biochemical and genetic characteristics of variegate porphyria in Italy. *Cell. Mol. Biol.* **55,** 79–88
14. Bonnin, A., Picornell, A., Orfila, J., Castro, J. A., and Ramon, M. M. (2009) Clinic and genetic evaluation of variegate porphyria (VP) in a large family from the Balearic Islands. *J. Inherit. Metab. Dis.* **32,** S59-S66
15. Rossetti, M. V., Granata, B. X., Giudice, J., Parera, V. E., and Batlle, A. (2008) Genetic and biochemical studies in Argentinean patients with variegate porphyria. *BMC Med. Genet.* **9,** 54
16. Warnich, L., Kotze, M. J., Groenewald, I. M., Groenewald, J. Z., van Brakel, M. G., van Heerden, C. J., de Villiers, J. N., van de Ven, W. J., Schoenmakers, E. F., Taketani, S., and Retief, A. E. (1996) Identification of three mutations and associated haplotypes in the protoporphyrinogen oxidase gene in South African families with variegate porphyria. *Hum. Mol. Genet.* **5,** 981–984
17. Meissner, P. N., Dailey, T. A., Hift, R. J., Ziman, M., Corrigall, A. V., Roberts, A. G., Meissner, D. M., Kirsch, R. E., and Dailey, H. A. (1996) A R59W mutation in human protoporphyrinogen oxidase results in decreased enzyme activity and is prevalent in South Africans with variegate porphyria. *Nat. Genet.* 13, 95–97
18. Arnould, S., and Camadro, J. M. (1998) The domain structure of protoporphyrinogen oxidase, the molecular target of diphenyl ether-type herbicides. *Proc. Natl. Acad. Sci. U.S.A.* **95,** 10553–10558
19. Haworth, P., and Hess, F. D. (1988) The generation of singlet oxygen ($^1O_2$) by the nitrodiphenyl ether herbicide oxyfluorfen is independent of photosynthesis. *Plant. Physiol.* **86,** 672–676
20. Kirsch, R. E., Meissner, P. N., and Hift, R. J. (1998) Variegate porphyria. *Semin. Liver. Dis.* **18,** 33–41
21. Maneli, M. H., Corrigall, A. V., Klump, H. H., Davids, L. M., Kirsch, R. E., and Meissner, P. N. (2003) Kinetic and physical characterisation of recombinant wild-type and mutant human protoporphyrinogen oxidases. *Biochim. Biophys. Acta* **1650,** 10–21
22. Qin, X., Tan, Y., Wang, L., Wang, Z., Wang, B., Wen, X., Yang, G., Xi, Z., and Shen, Y. (2011) Structural insight into human variegate porphyria disease. *FASEB J.* **25,** 653–664
23. Shepherd, M., and Dailey, H. A. (2005) A continuous fluorimetric assay for protoporphyrinogen oxidase by monitoring porphyrin accumulation. *Anal. Biochem.* **344,** 115–121
24. Sun, L., Wen, X., Tan, Y., Li, H., Yang, X., Zhao, Y., Wang, B., Cao, Q., Niu, C., and Xi, Z. (2009) Site-directed mutagenesis and computational study of the Y366 active site in Bacillus subtilis protoporphyrinogen oxidase. *Amino Acids* **37,** 523–530
25. Qin, X., Sun, L., Wen, X., Yang, X., Tan, Y., Jin, H., Cao, Q., Zhou, W., Xi, Z., and Shen, Y. (2010) Structural insight into unique properties of protoporphyrinogen oxidase from *Bacillus subtilis*. *J. Struct. Biol.* **170,** 76–82
26. Otwinowski, Z., and Minor, W. (1997) Processing of X-ray diffraction data collected in oscillation mode. pp 307–326, Elsevier, Boston, MA
27. McCoy, A. J. (2007) Solving structures of protein complexes by molecular replacement with phaser. *Acta Crystallogr. D Biol. Crystallogr.* **63**, 32–41
28. Emsley, P., and Cowtan, K. (2004) Coot: model-building tools for molecular graphics. *Acta Crystallogr. D Biol. Crystallogr.* **60**, 2126–2132
29. Brünger, A. T., Adams, P. D., Clore, G. M., DeLano, W. L., Gros, P., Grosse-Kunstleve, R. W., Jiang, J. S., Kuszewski, J., Nilges, M., Pannu, N. S., Read, R. J., Rice, L. M., Simonson, T., and Warren, G. L. (1998) Crystallography & NMR system: a new software suite for macro-molecular structure determination. *Acta Crystallogr. D Biol. Crystallogr.* **54**, 905–921
30. Laskowski, R. A., MacArthur, M. W., Moss, D. S., and Thornton, J. M. (1993) PROCHECK: a program to check the stereochemical quality of protein structures. *J. Appl. Crystallogr.* **26,** 283–291
31. Case, D. A., Cheatham, T. E., 3rd, Darden, T., Gohlke, H., Luo, R., Merz, K. M., Jr., Onufriev, A., Simmerling, C., Wang, B., and Woods, R. J. (2005) The Amber biomolecular simulation programs. *J. Comput. Chem.* **26,** 1668–1688
32. Duan, Y., Wu, C., Chowdhury, S., Lee, M. C., Xiong, G., Zhang, W., Yang, R., Cieplak, P., Luo, R., Lee, T., Caldwell, J., Wang, J., and Kollman, P. (2003) A point-charge force field for molecular mechanics simulations of proteins based on condensed-phase quantum mechanical calculations. *J. Comput. Chem.* **24,** 1999–2012

33. Lee, M. C., and Duan, Y. (2004) Distinguish protein decoys by using a scoring function based on a new AMBER force field, short molecular dynamics simulations, and the generalized born solvent model. *Proteins* **55,** 620–634
34. Frisch, M. J., Trucks, G. W., Schlengel, H. B., Scuseria, G. E., Robb, M. A., Cheeseman, J. R., Zakrzewski, V. G., Montgomery, J. A., Jr., Stratman, R. E., Burant, J. C., Dapprich, S., Millam, J. M., Daniels, A. D., Kundin, K. N., Strain, M. C., Farkas, O., Tomasi, J., Barone, V., Cossi, M., Cammi, R., Mennucci, B., Pomelli, C., Adamo, C., Clifford, S., Ochterski, J., Petersson, G. A., Ayala, P. Y., Cui, Q., Morokuma, K., Malick, D. K., Rabuck, A. D., Raghavachari, K., Foresman, J. B., Ciolowski, J., Ortiz, J. V., Stefanov, B. B., Liu, G., Liashebko, A., Piskorz, P., Komaromi, I., Gomperts, R., Martin, R. L., Fox, D. J., Keith, T., Al-Laham, M. A., Peng, C. Y., Nanayakkara, A., Gonzalez, C., Challacombe, M., Grill, P. M. W., Johnson, B., Chen, W., Wong, M. W., Andres, J. L., Head-Gordon, M., Replogle, E. S., and Pople, J. A. (2004) *Gaussian 03*, Revision C.01, Gaussian, Inc., Wallingford, CT
35. Darden, T., York, D., and Pedersen, L. (1993) Particle Mesh Ewald: an NLog(N) method for Ewald sums in large systems. *J. Chem. Phys.* **98,** 10089–10092
36. Ryckaert, J. P., Ciccotti, G., and Berendsen, H. J. (1977) Numerical integration of the cartesian equations of motion of a system with constraints: molecular dynamics of *n*-Alkanes. *J. Comput. Phys.* **23,** 327–341
37. Akhtar, M. (1991) *Biosynthesis of Tetrapyrroles*, pp. 67–99, Elsevier, Amsterdam
38. Fraaije, M. W., and Mattevi, A. (2000) Flavoenzymes: diverse catalysts with recurrent features. *Trends. Biochem. Sci.* **25,** 126–132
39. Post, C. B., Young, L., and Zheng, J. (1994) Conformational equilibrium of dihydronicotin amide in LDH-NADH. *Pure Appl. Chem.* **66,** 83–88
40. Lightstone, F. C., and Bruice, T. C. (1996) Ground state conformations and entropic and enthalpic factors in the efficiency of intramolecular and enzymatic reactions. 1. cyclic anhydride formation by substituted glutarates, succinate, and 3,6-endoxo-Δ4-tetrahydrophthalate monophenyl esters. *J. Am. Chem. Soc.* **118,** 2595–2605
41. Corrigall, A. V., Hift, R. J., Davids, L. M., Hancock, V., Meissner, D., Kirsch, R. E., and Meissner, P. N. (2000) Homozygous variegate porphyria in South Africa: genotypic analysis in two cases. *Mol. Genet. Metab.* **69,** 323–330
42. Corrigall, A. V., Hift, R. J., Davids, L. M., Hancock, V., Meissner, D., Kirsch, R. E., and Meissner, P. N. (2001) Identification of the first variegate porphyria mutation in an indigenous black south African and further evidence for heterogeneity in variegate porphyria. *Mol. Genet. Metab.* **73,** 91–96
43. Jones, C., Jordan, P. M., and Akhtar, M. (1984) Mechanism and stereochemistry of the porphobilinogen deaminase and protoporphyrinogen IX oxidase reactions: stereospecific manipulation of hydrogen atoms at the four methylene bridges during the biosynthesis of haem. *J. Chem. Soc. Perkin Trans.* **1,** 2625–2633
44. Jones, C., Jordan, P. M., Chaudhary, A. G., and Akhtar, M. (1979) Stereospecificity of hydrogen removal from the four methylene bridges in haem biosynthesis: specific incorporation of the 11 pro-S hydrogen of porphobilinogen into haem. *J. Chem. Soc. Chem. Commun.* **0,** 96–97
45. Koch, M., Breithaupt, C., Kiefersauer, R., Freigang, J., Huber, R., and Messerschmidt, A. (2004) Crystal structure of protoporphyrinogen IX oxidase: a key enzyme in haem and chlorophyll biosynthesis. *EMBO J.* **23,** 1720–1728
46. Bruice, T. C., and Lightstone, F. C. (1999) Ground state and transition state contributions to the rates of intramolecular and enzymatic reactions. *Acc. Chem. Res.* **32,** 127–136
47. Seeman, J. I. (1983) Effect of conformational change on reactivity in organic chemistry. Evaluations, applications, and extensions of Curtin-Hammett Winstein-Holness kinetics. *Chem. Rev.* **83,** 83–134
48. Bruice, T. C., and Benkovic, S. J. (2000) Chemical basis for enzyme catalysis. *Biochemistry* **39,** 6267–6274
49. Lau, E. Y., and Bruice, T. C. (1998) Importance of correlated motions in forming highly reactive near attack conformations in catechol *O*-methyltransferase. *J. Am. Chem. Soc.* **120,** 12387–12394
50. Hur, S., and Bruice, T. C. (2003) The near attack conformation approach to the study of the chorismate to prephenate reaction. *Proc. Natl. Acad. Sci. U.S.A.* **100,** 12015–12020
51. Kiss, G., Röthlisberger, D., Baker, D., and Houk, K. N. (2010) Evaluation and ranking of enzyme designs. *Protein Sci.* **19,** 1760–1773
52. Luo, J., and Bruice, T. C. (2001) Dynamic structures of horse liver alcohol dehydrogenase (HLADH): results of molecular dynamics simulations of HLADH-NAD^+-$PhCH_2OH$, HLADH-NAD^+-$PhCH_2O^-$, and HLADH-NADH-PhCHO. *J. Am. Chem. Soc.* **123,** 11952–11959
53. Bruice, T. C. (2006) Computational approaches: Reaction trajectories, structures, and atomic motions. Enzyme reactions and proficiency. *Chem. Rev.* **106,** 3119–3139